Check for updates

Efficient tuning of zinc phthalocyanine-based dyes for dye-sensitized solar cells: a detailed DFT study†

Sabir Ali Siddique,[a] Muhammad Arshad, [ID] *[b] Sabiha Naveed,[a] Muhammad Yasir Mehboob, [ID] [c] Muhammad Adnan, [ID] [d] Riaz Hussain,*[c] Babar Ali,[e] Muhammad Bilal Ahmed Siddique*[f] and Xin Liu [ID] *[g]

The growing energy demand speed up the designing of competent photovoltaic materials. Herein, five zinc phthalocyanine-based donor materials **T1–T5** are designed by substituting various groups (isopropoxy, cyano, fluoro, methoxycarbonyl, and dicyanomethyl) around zinc phthalocyanine. B3LYP/6-31G (d,p) level density functional theory (DFT) was used to investigate the optoelectronic properties of five zinc phthalocyanine-based dyes **T1–T5** for dye-sensitized solar cells. The designed molecule **T1** shows maximum absorption wavelength (λ_{max}) in the absorption spectrum at 708.89 and 751.88 nm both in gaseous state and in THF (tetrahydrofuran) solvent. The E_g value of **T1** (1.86 eV) is less than reference **R**, indicating a greater charge transfer rate for **T1** among the molecules. The values of open-circuit voltages achieved with acceptor polymer PC$_{71}$BM are higher than **R** except for **T1** and are 0.69 V, 1.95 V, 1.20 V, 1.44 V, and 1.84 V for **T1**, **T2**, **T3**, **T4**, and **T5**, respectively. The lower the reorganization energy, the higher the charge transfer for **T1** due to its lower hole mobility (0.06297 eV) than **R**. Thus, the designed **T1–T5** molecules are expected to exhibit superior performance in dye-sensitized solar cells.

Introduction

Dye-sensitized solar cells (DSSCs) have originated as an economically credible photovoltaic technology and are considered a promising alternative to conventional p–n junction devices.[1] Since they have already demonstrated their worth for the society by providing more than 13% power conversion efficiency (PCE) at the laboratory scale, while around 10% in small photovoltaic modules.[2] Due to the remarkable achievements under various irradiation conditions, DSSCs are considered an ideal candidate under artificial light, shadowed or dim environments.[3] Their manufacturing process is quite simple, cost-

effective, environmentally friendly, and compatible to meet the industrial requirements to produce large-area devices.[4]

However, during the preparation of transparent SCs, there is a need for a compromise between the efficiency and transparency of devices. Therefore, a lot of efforts have been made to overcome the issue and prepare state-of-the-art devices beyond the limit of fixing optical transmissions while fabricating semi-transparent DSSCs devices. Primarily, the ruthenium-based DSSCs offered good optical and photovoltaic characteristics and are quite prominent as compared with previously used DSSCs, but their usage was limited due to very small absorption in the near-infrared region with lower intensities.[5] Therefore, due to this, another family of dyes, such as phthalocyanines, offered good and efficient absorption properties when used in DSSCs because of their integrated structure and charge shifting behavior.[6]

In recent years, the use of phthalocyanines is quite attractive due to their specific merits such as they are electrochemically, photo-chemically, thermally stable species, and this is because of their higher absorption capability in the near and far-infrared region.[7] Importantly, absorption in the near-infrared region with maximum intensity is associated with phthalocyanines when used in DSSCs. The light absorption bands in phthalocyanines are shifted towards the red/infrared region of radiations due to the positioning of peripheral and non-peripheral functional groups on the macrocycle.

In phthalocyanines, Zn-phthalocyanines are the successful candidates for DSSCs because of electron-donating units, which

[a]*Center for Organic Chemistry, School of Chemistry, University of the Punjab, Lahore-54590, Pakistan*

[b]*Institute of Chemistry, The Islamia University of Bahawalpur, Baghdad-ul-Jadeed Campus, Bahawalpur-63100, Pakistan. E-mail: muhammad.arshad@iub.edu.pk*

[c]*Department of Chemistry, University of Okara, Okara-56300, Pakistan. E-mail: riazhussainansari@gmail.com*

[d]*Graduate School, Department of Chemistry, Chosun University, 501-759 Gwangju, Republic of Korea*

[e]*Department of Physics, University of Okara, Okara-56300, Pakistan*

[f]*School of Chemistry and Chemical Engineering, Shandong University, Jinan-250100, China. E-mail: bilal.siddique@mail.sdu.edu.cn*

[g]*State Key Laboratory of Fine Chemicals, Department of Chemistry, Dalian University of Technology, Dalian, 116024, P. R. China. E-mail: xliu@dlut.edu.cn*

† Electronic supplementary information (ESI) available: Supporting information contains figures and tables of our studied compounds. See DOI: 10.1039/d1ra04529f

are the key constituents on the macrocycle. Three electron donor units are on the isoindole sub-unit (named as A) of the macrocycle, while the fourth unit is present on the anchoring group that directly interacts with metal oxide.[8] This A3B type configuration of Zn-phthalocyanines allows less steric hindrance with efficient push–pull effects making Zn-phthalocyanines an efficient absorber of sunlight in the near-infrared region.[9,10]

In the literature, studies disclosed the presence of substituents on A and B units, like electron-rich unit (2,6-bis(*n*-butoxy) phenoxy) group on A and electron catching group such as COOH on B that directly boosted PCEs up to 6.4%, which is more than reported previously by Nazeeruddin.[11] Besides these reports, research is going on in this field with continuous increments in PCE values. Recently, Milan and his co-authors efficiently designed and demonstrated Zn-phthalocyanines for DSSCs.[12] They studied peripherally substituted push–pull Zn-phthalocyanines bearing three electron-donating diphenylamine substituents and a carboxylic acid anchoring group and integrated it as a sensitizer in TiO2-based DSSCs. They concluded that the synthesized molecule offered great absorption in the near-infrared region, which directly enhanced the light-harvesting efficiencies.

In DSSC, sensitizers with extended absorption in the near IR region of the solar emission spectrum are essential, and phthalocyanines are excellently suitable for their integration in light energy conversion systems. Therefore, asymmetric Zn-phthalocyanine is being adapted as a standard material showing exceptional light to energy efficiency in DSSCs. The asymmetric phthalocyanines with higher light-harvesting effects result in higher photocurrents and their potential use.[13–15] The recent studies highlight tetra triphenylamine-substituted Zn-phthalocyanine as a hole transporting material and highlight the importance of a buffer layer between the perovskite layer and the hole-transporting layer.[16]

Herein, we designed a new strategy to further improve the absorption/light-harvesting capabilities of Zn-phthalocyanines by incorporation of different end-capped units. With these modifications, we efficiently designed five new molecules that offer high absorption in the near-infrared region with maximum intensity. After designing, we theoretically characterized these materials by computing geometric parameters and physicochemical properties. Moreover, the density of states analysis, alignment of frontier molecular orbitals, reorganizational energy of holes and electrons, transition density matrix, and photovoltaic properties of these newly designed materials are investigated. The outcome from all theoretical parameters suggested that these designed molecules are good candidates for high-performance DSSCs applications.

Computational details

All the computations were carried out on designed molecules as well as the reference molecule using the Gaussian 09 package.[17] The structures of molecules were drawn with the help of Gauss View 6.0.[18] Initially, the absorption spectra and geometry of reference compound R[19] were optimized using CAM-B3LYP,

B3LYP, WB97XD MPW1PW91, HSEH1PBE, PBEPBE, and TPSSTPSS functionals with 6-31G (d,p) basis set and the results compared with experimental data. B3LYP at 6-31G (d,p) basis set provides the strongest agreement between experimental and theoretical results. Thus, this method was selected for further calculations. Both the electronic and optical properties like the density of states, maximum absorption (λ_{max}), frontier molecular orbitals (FMOs), transition density matrix (TDMs), and reorganization energy are calculated using the B3LYP/6-31G (d,p) method of DFT.

Open circuit voltages (V_{oc}) explain the amount of current that can be passed through any material. The difference between HOMO$_{donor}$ and LUMO$_{acceptor}$ is known as open-circuit voltage. Reorganization of energy is the main point of charge mobilities. There are two parts of reorganization energy, internal and external. Relaxation in the environment is studied with the help of external reorganization (λ_h), and change in molecular geometry is studied with internal reorganization (λ_e). In this study, we only deal with internal reorganization (λ_e).[20] The equations of reorganization energies are as following:

$$\lambda_e = [E_0^- - E_-] + [E_-^0 - E_0] \tag{1}$$

$$\lambda_h = [E_0^+ - E_+] + [E_+^0 - E_0] \tag{2}$$

In the above equations, E_-^0 and E_+^0 are the energies of neutral molecules at the anionic and cationic states, respectively. E_+, E_- indicates the energies of cation and anion, respectively, *via* optimized geometries of cation and anion molecules. E_0^+ and E_0^- are the energies of cation and anion with the optimized structure of neutral molecules. Finally, E_0 is the energy of neutral molecules at the ground state.

Results and discussion

In the present study, B3LYP, ωB97XD, MPW1PW91, CAM-B3LYP, HSEH1PBE, PBEPBE, and TPSSTPSS functionalities with 6-31G (d,p) basis set were applied for initial optimization of the reference molecule R to determine the optoelectronic properties. The maximum absorption (λ_{max}) values of reference R with B3LYP, ωB97XD, MPW1PW91, CAM-B3LYP, HSEH1PBE, PBEPBE, and TPSSTPSS are found to be: 708.24 nm, 635.13 nm, 681.83 nm, 645.15 nm, 716.22 nm, 895.52 nm, and 863.52 nm, respectively. The λ_{max} of reference R obtained experimentally is 711 nm [19] and shown in Fig. 1. The B3LYP/6-31G (d,p) method of DFT has the strongest relationship with the experimental λ_{max} value and it is therefore ideal for further calculations of designed molecules T1–T5.

This report aims to improve the photovoltaic properties of zinc phthalocyanine-based donors *via* modification of donor moieties. For this, a newly synthesized molecule, (23-carboxy-2,9,16-tris(diphenylamino)phthalocyanine-29-yl)zinc(II) complex R[19] is modified using specific donor groups like (isopropoxy, cyano, fluoro, methoxycarbonyl, and dicyanomethyl). The modified structures of all newly designed molecules T1–T5 and reference R are expressed in Fig. 2. Effective molecular design is the key to boosting photovoltaic efficiency by decreasing the energy gap (E_g) by operating charge transfer (CT)
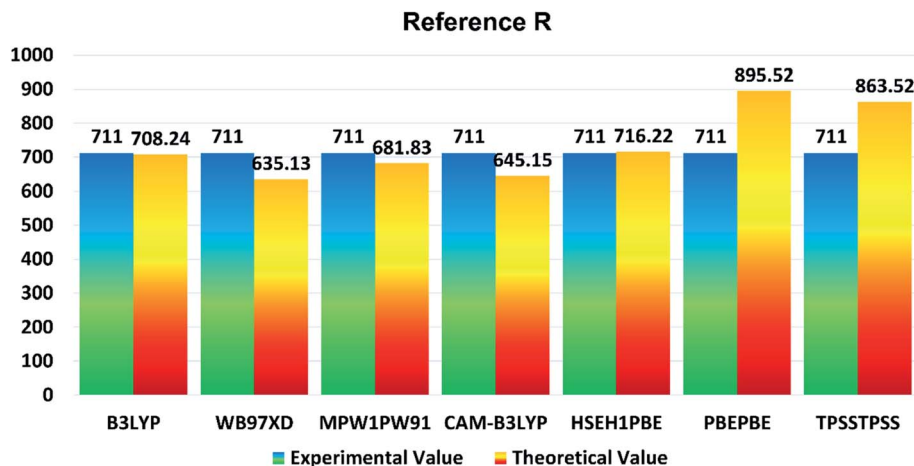
Reference R

Fig. 1 Comparison diagram of λ_{max} of R between experimental and theoretical values with B3LYP, MPW1PW91, CAM-B3LYP, ωB97XD, HSEH1PBE, PBEPBE and TPSSTPSS at 6-31G (d,p).

within the molecule and regulating its energy levels. The optimization of the ground state and the planar conformation of optimized structures of the reference **R** and designed molecules **T1–T5** are shown in Fig. S1,† and it shows that the planar conformations promote the mobility of charges in molecules (**T1, T2, T3, T4**, and **T5**) due to increased conjugation present in these systems by the delocalization of electrons.

The photovoltaic efficiency of organic solar cells can be improved by a small energy gap (E_g). The HOMO and LUMO of molecular orbitals clarify the bonding and anti-bonding character of compounds.[21] The amount of current, voltage, and effectiveness of the cell is directly proportional to the transfer of electrons from the donor part to the acceptor part of the molecule. The transfer of electrons depends on the method of
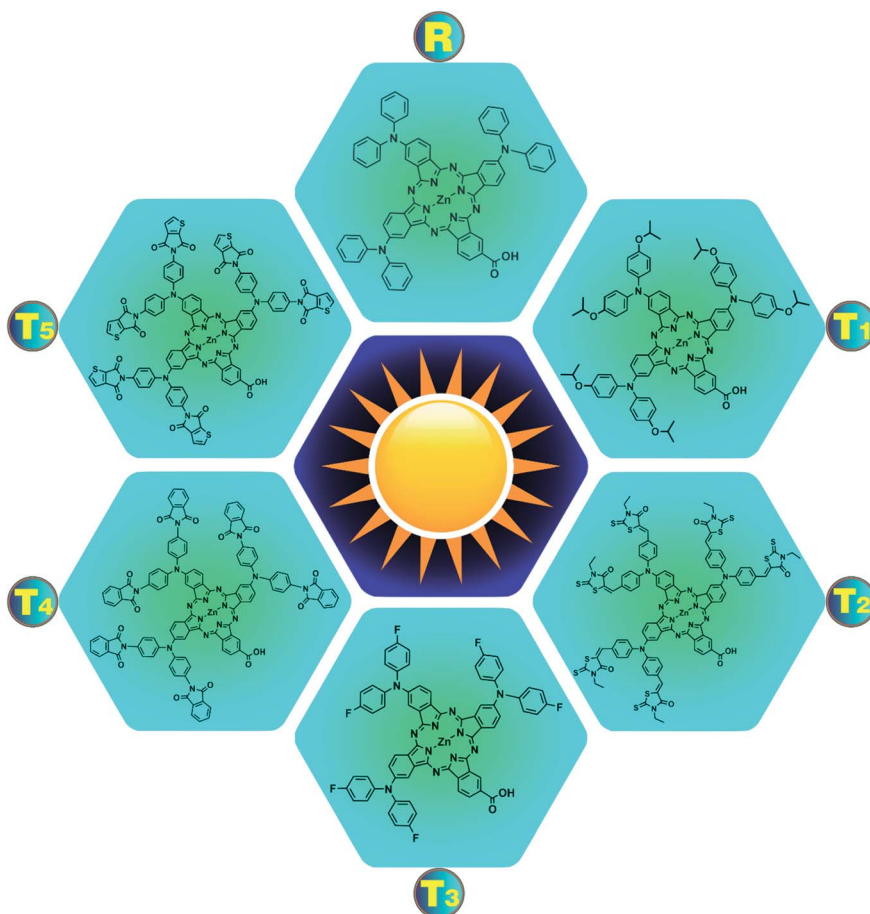

Fig. 2 Structural formulas of reference compound R and designed molecules T1–T5.
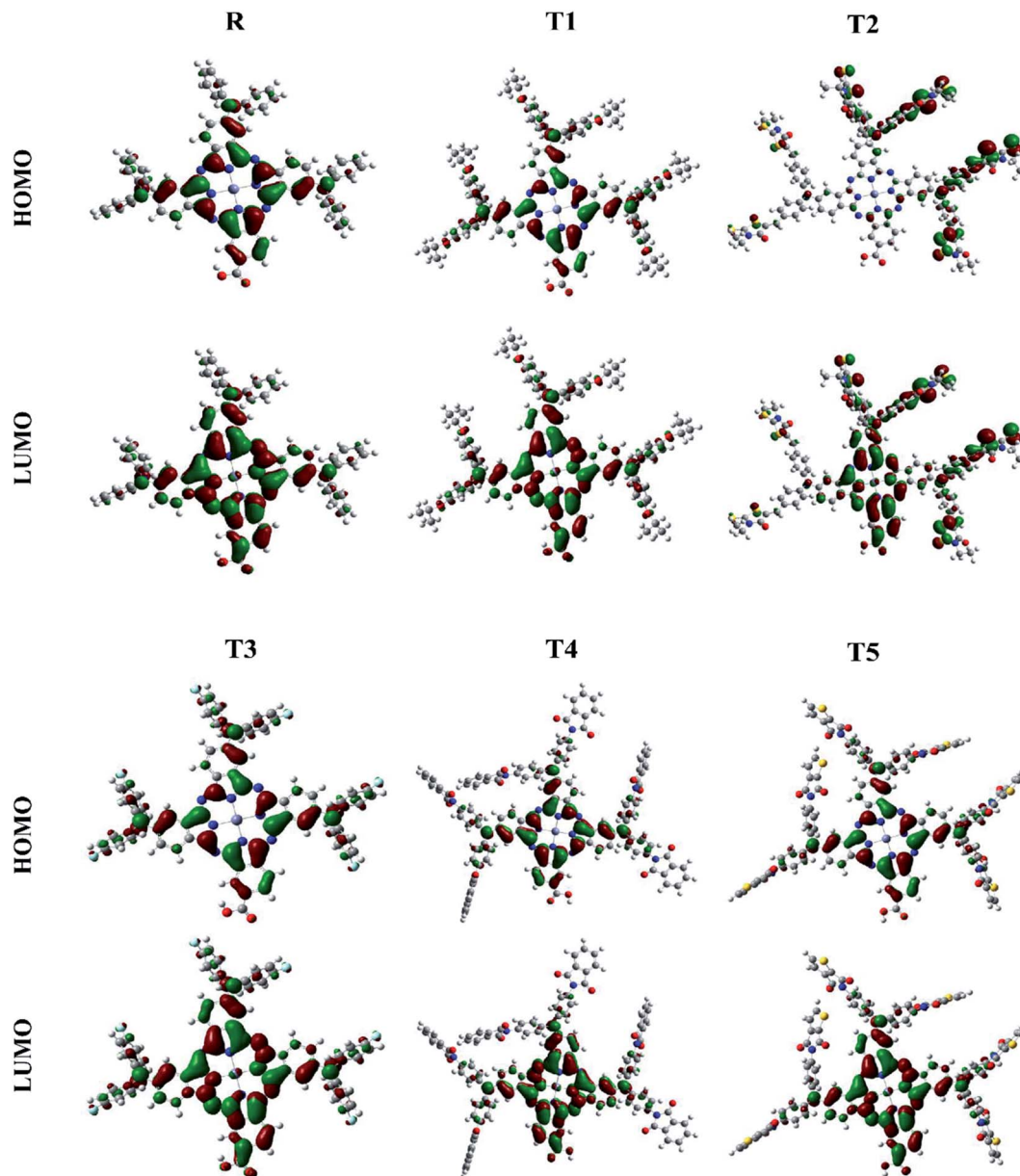
Fig. 3 Frontier molecular orbital diagrams of reference **R** and compounds **T1–T5** at B3LYP/6-31G (d,p) level of theory.

electron excitation. Thus, the transfer of an electron from the donor to the acceptor can be improved by improving the method of electron excitation.[22] In Fig. 3, frontier molecular orbitals of compounds are represented as a distribution around HOMO and LUMO. The reference **R** and **T1–T5** molecules were optimized with B3LYP at the 6-31G (d,p) basis set level. The calculated band gap (E_g) values between HOMO and LUMO are set as a stability index and correspond to the difference between HOMO–LUMO energies.[23]

To avoid self-aggregation, the donor and acceptor parts of the newly designed compounds were set in the 3D method. The electronic and optical characteristics of molecules **T1–T5** were characterized by frontier molecular orbital theory distribution. The E_{HOMO} and E_{LUMO} of the molecule **R** were −4.76 and −2.82 eV, respectively, and the band gap was 1.94 eV, as shown

in Table 1. The E_{HOMOs} and E_{LUMOs} of new compounds **T1, T2, T3, T4, T5** were −4.39, −5.34, −4.90, −4.57, −4.60 eV, and −2.53, −3.45, −2.97, −2.69, −2.80 eV, respectively, as described in Fig. 4. Besides the significance of HOMO and LUMO energies, their band gaps are also important. The band gap value of compound **R** was 1.94 eV, while **T5** has the lowest (1.80 eV) band gap than all other molecules due to the isopropoxy group bearing the donor characteristics.

The E_g values of the five newly designed compounds are 1.86, 1.89, 1.93, 1.87, 1.80 eV, respectively. The **T5** molecule has the lowest band gap than reference molecule **R**, which means this molecule can display an easy charge transformation method. Comparatively low HOMO values of designed compounds will accelerate the open-circuit voltage of dye-sensitized solar cells.

Table 1 Energies of HOMOs and LUMOs and HOMO–LUMO gap at B3LYP/6-31G (d,p) level of theory for reference compound **R** and designed molecules **T1**, **T2**, **T3**, **T4**, and **T5**

Molecules	E_{HOMO} (eV)	E_{LUMO} (eV)	E_g (eV)
R	−4.76	−2.82	1.94
T1	−4.39	−2.53	1.86
T2	−5.34	−3.45	1.89
T3	−4.90	−2.97	1.93
T4	−4.57	−2.69	1.87
T5	−4.60	−2.80	1.80

Density of state (DOS) and overlap population density of state (OPDOS)

To obtain details on the increase in energy levels per unit, OPDOS and DOS studies of all the newly planned compounds were performed, and their results support the findings obtained from the frontier molecular orbitals given in Fig. 3. The higher value of DOS is that there are a significant number of states for these energy levels. The zero values of OPDOS and DOS indicate that there is no state available to occupy the electrons for this level of energy.[24,25]

Generally, DOS represents the space occupied by the system. DOS and OPDOS for molecules **T1–T5** and reference **R** at B3LYP/6-31G (d,p) method of DFT are given in Fig. 5 and 6, respectively. OPDOS and DOS studies help clarify the contribution of donor–acceptor species in the formation of frontier molecular orbitals. DOS study illustrates the energy of occupied and unoccupied MO's of designed molecules. In the spectrum, green and blue colors represent the energy states to occupy for the electron around the donor part of the compound, while red color defines the acceptor moiety.

In the graph of density of state, the space between the acceptor and donor part of the compound is represented by the band gap (E_g). The band gap is the energy needed for electron excitation.[26] In this study, smaller energy is required to excite the electrons from the acceptor to the donor part for all the compounds.

Optical properties

The optical characteristics of photovoltaic compounds (**T1–T5**) were predicted with the TD-B3LYP/6-31G (d,p) method of DFT

and are given in Table 2. The design feature of effective photovoltaic compounds is based on their strong and comprehensive absorption properties. Firstly, to observe the photophysical properties in both the gaseous and **THF** solvent phases, molecule **R** was optimized with different functionals like TD-ωB97XD, TD-B3LYP, TD-CAMB3LYP, TD-MPW1PW91, TD-HSEH1PBE, TD-PBEPBE, and TD-TPSSTPSS at 6-31G (d,p) method of DFT.

In comparison, the results obtained from the TD-B3LYP/6-31G (d,p) DFT method were consistent with the experimental UV spectra of compound **R**. The theoretical study exposed that the absorption spectrum (λ_{max}) of the reference compound in **THF** solvent was 708.24 nm and 680.11 nm in the gaseous phase. The experimental absorption value of the reference compound was 711 nm that is similar to the value obtained in **THF** solvent. Therefore, we used the TD-B3LYP/6-31G (d,p) method to compute the photophysical characteristics of all the newly designed compounds **T1–T5**. For all these compounds and reference **R**, 10 **ETS** (electronic transition excited states) were generated in **THF** solvent as well as in the gaseous phase. The experimental wavelength (λ_{max}), calculated wavelength (λ_{max}), oscillator strength (f), %ETC (electron transport contribution), dipole moment, and excitation energy (E_x) for all compounds **T1–T5** at TD-B3LYP/6-31G (d,p) method of DFT in the gas and solvent (**THF**) phases are shown in Table 2. The calculated λ_{max} in the gas phase for designed compounds **T1–T5** and reference **R** at TD B3LYP/6-31G (d,p) was in the range of 652.34–708.89 nm, as shown in Fig. 7.

The compounds **T1–T5** and reference **R** display strong and broad spectral peaks, ranging from 600 nm to 1000 nm. Both the designed and reference molecules display one large peak in the range from 600 to 900 nm. The molecule **T1** has shown higher λ_{max} than reference **R** in the gaseous phase. With an oscillator strength of 0.64, the λ_{max} of reference **R** was 680.11 nm in the gaseous phase. For the **T1** molecule, the absorption band is red-shifted than **T2**, **T3**, **T4**, and **T5** designed molecules with increased oscillator strength (f) up to 0.70. The obtained oscillator strengths (f) of **T1**, **T2**, **T3**, **T4**, and **T5** molecules were 0.69, 0.71, 0.65, 0.76, and 0.42, respectively.
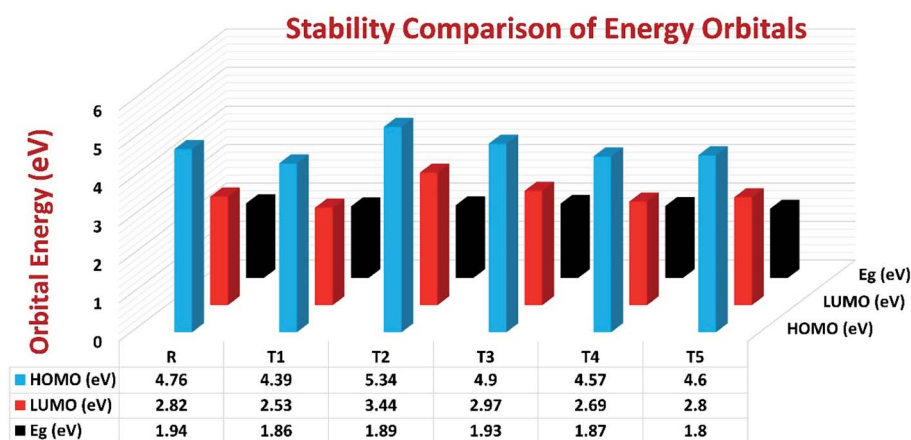

Fig. 4 Orbital energies of designed donor molecules **T1–T5** and reference molecule **R** at B3LYP/6-31G (d,p) level of theory.
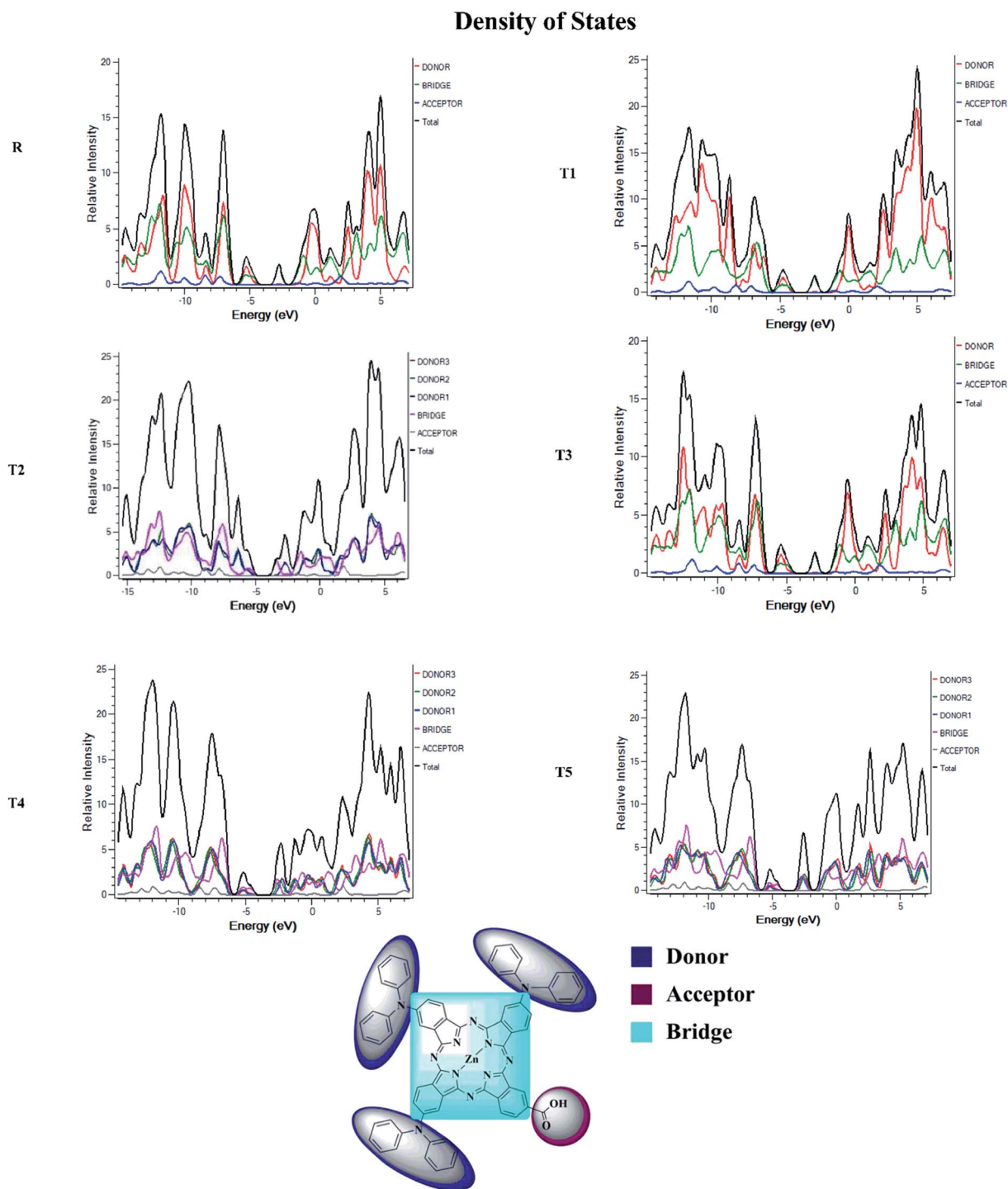
Density of States

Fig. 5 DOS map for reference **R** and molecules **T1–T5** at B3LYP/6-31G (d,p) level of theory.

The compound **T5** is blue-shifted in the ultraviolet-visible spectrum at the lowest oscillator strength 0.42 with λ_{max} 682.88 nm than compound **R**. The electron transport contributions percentage (%ETC) in both phases, gaseous and solvent, changes from 81% to 94% and 93% to 96%, respectively. If the %ETC is smaller, excitation chances will be greater for **T1–T5** designed molecules. Among all newly designed molecules, **T2** and **T5** have lower %ETC values both in gaseous and solvent phases, lower than the reference compound in both phases. The chances for the excitation of electrons of **T2** and **T5** are greater due to lower %ETC.

Molecular electrostatic potential

Molecular ESP calculations were performed to compare rich and deficient sites of electrons in **T1–T5** designed molecules
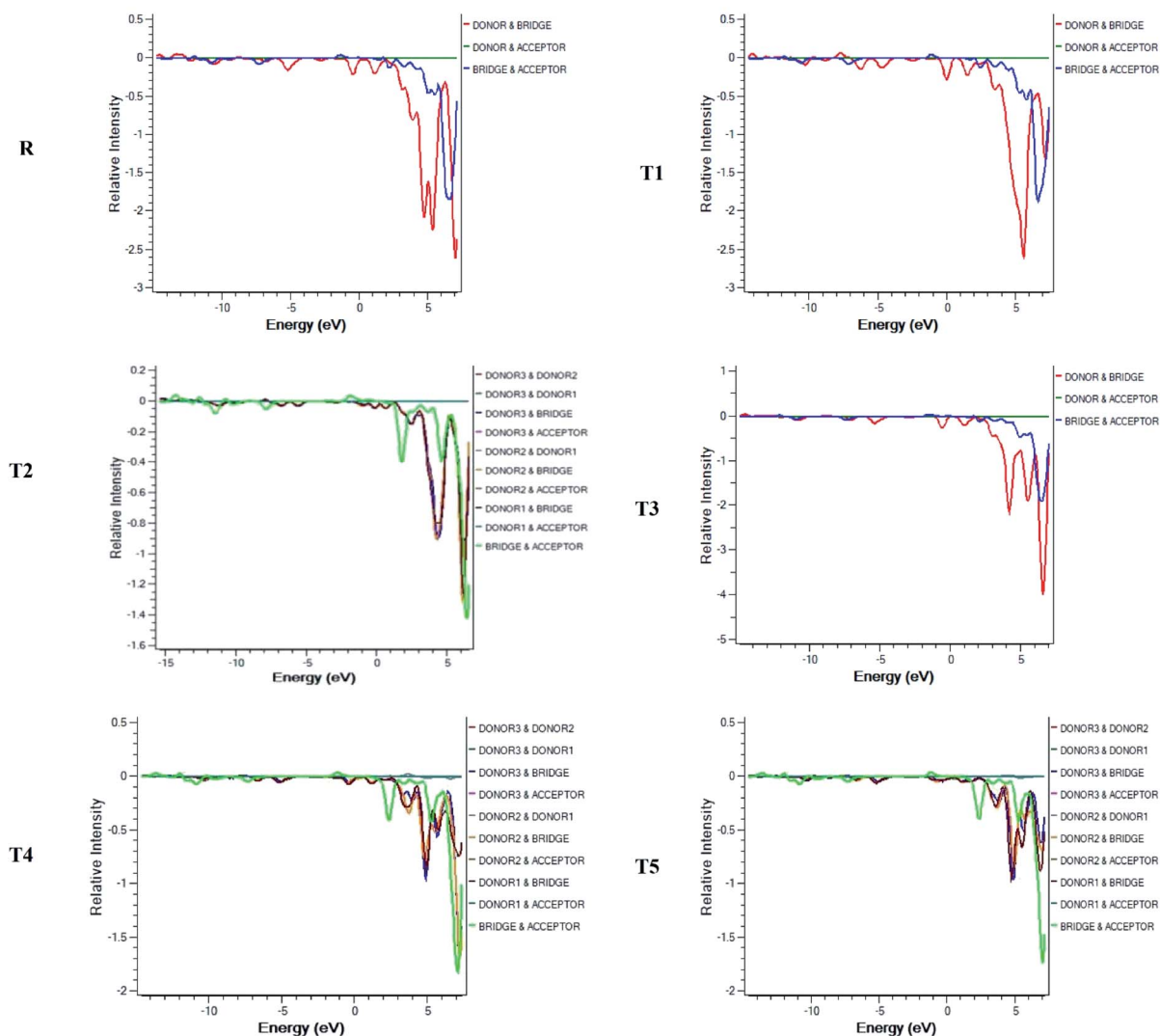
Overlap Density of States

Fig. 6   OPDOS map for reference **R** and molecules **T1–T5** at B3LYP/6-31G (d,p) level of theory.

with reference **R**. The properties of the compounds were represented by three colors (green, red, blue) in the MEP graphs. The green color shows the neutral, the blue color indicates the positive charge accumulation (electron-efficient) part, and red represents the negatively charged accumulation (electron-deficient) part of the compound.[27]

Interestingly, it was observed that the distribution pattern of all compounds, as well as reference, was the same that indicates all the designed compounds can be used for solar cells. Therefore, all newly designed molecules are the best candidates for solar cell applications due to similar MEP graphic distribution to the **R** reference molecule (Fig. 8).

Reorganization energy

Dye-sensitized solar cell performance relies on the charge mobilities. The reorganization energies of electron (λ_e) and hole (λ_h) mobilities help to calculate the charge mobilities. The

evaluation of the relation between the transportation of charges and the structure of molecules is important for the improvement of photovoltaic materials. The reorganization energy has an inverse relationship with the mobilities of charges. As the value of reorganization energy is higher, lower will be the mobility of charges of the newly designed compounds.

For the analysis of reorganization energies of reference **R** and compounds **T1–T5**, the geometries of the anions and cations were used. The values for reorganization energy of all the molecules as well as reference are given in Table 3. This analysis suggests that the designed compound **T4** has better λ_e than the reference and other designed compounds due to isoindoline-1,3-dione substituent. The reorganization energy value of λ_h as compared to λ_e indicates **T1** is good for the mobility of charges. The λh value of the reference is greater than the designed donor compound **T1**, which means that the mobility of charges of the reference is lower than the **T1** compound. The

Table 2 Calculated wavelength (λ_{max}), experimental wavelength (λ_{max}), excitation energies (E_x) and oscillator strength (f), dipole moment (μ), % electron transport contributions (%ETC) of reference **R** and designed molecules **T1**, **T2**, **T3**, **T4**, and **T5** at B3LYP/6-31G (d,p) level of theory in the gas and solvent phases, respectively

	Molecules	Calc. λ_{max} (nm)	Exp. λ_{max} (nm)	f (a.u)	Assignment	E_x (eV)	Dipole moment (debye)
Gaseous	**R**	680.11	711	0.64	HOMO → L+1 (93%)	1.823	8.511
	T1	708.89	—	0.69	HOMO → L+1 (94%)	1.749	11.875
	T2	708.93	—	0.71	HOMO → LUMO (63%),	1.749	5.861
					HOMO → L+1 (30%)		
	T3	678.51	—	0.65	HOMO → L+1 (93%)	1.827	6.942
	T4	671.16	—	0.76	HOMO → L+1 (91%)	1.847	7.054
	T5	682.88	—	0.42	HOMO → L+1 (86%)	1.816	9.056
Solvent	**R**	708.24	711	0.81	HOMO → L+1 (96%)	1.751	10.007
	T1	751.88	—	0.82	HOMO → L+1 (96%)	1.649	14.073
	T2	706.46	—	0.97	HOMO → LUMO(58%),	1.755	8.515
					HOMO → L+1 (37%)		
	T3	706.38	—	0.81	HOMO → L+1 (96%)	1.755	8.469
	T4	697.95	—	0.94	HOMO → L+1 (95%)	1.776	8.763
	T5	695.17	—	0.87	HOMO → L+1 (95%)	1.783	10.919

values for electron mobilities λ_e for reference as well as other compounds **T1–T5** are 0.19217, 0.19631, 0.14933, 0.19986, 0.07197, and 0.20844 eV, correspondingly.

The newly designed compound **T2** has a lower value of λ_e than reference, which indicates this compound has greater mobility of charges than the reference compound. The mobility of holes λ_h for reference as well as other molecules **T1–T5** is 0.08712, 0.06297, 0.07883, 0.08122, 0.10100, 0.12448 eV, respectively. The **T1** molecule has a low value of λ_h than reference and other designed molecules. The least value of reorganizational energy of holes in the **T1** molecule suggested that the **T1** molecule is a potential candidate for efficient hole transport material. The analysis of reorganization energies proves that **T1** is the best for hole transport mobility.

Dipole moment

The solubility of dye-sensitized solar cell materials is mainly dipole moment dependent. Thus, the dipole moment is considered a key factor to enhance the performance of OSCs. The solubility is directly related to the dipole moment. When the value of the dipole moment is high, the solubility in organic solvents also increases and *vice versa*.[28] In polar solvents, the solubility of compounds increases by increasing the number of polar atoms in the structure of compounds.

The molecule **T2** shows the low value of dipole moment in both the gaseous phase and in solvent **THF**. DSSC's fabrication in the film is somehow affected by dipole moment. Two dipoles are present in such a fashion (anti-parallel), in which they stimulate molecular fabrication, which directly improved the crystallinity. Furthermore, it is said that a higher value of dipole moment increases the charge mobility. The higher value of dipole moment also reduces the disorder between acceptor and donor, resulting in the significantly increased value of charge mobility between acceptor and donor. So, low dipole moment allows low mobility and high stability in the designed molecule.[29] The dipole moments of **T1–T5** molecules and reference **R** in **THF** solvent were obtained with functionals B3LYP and TD
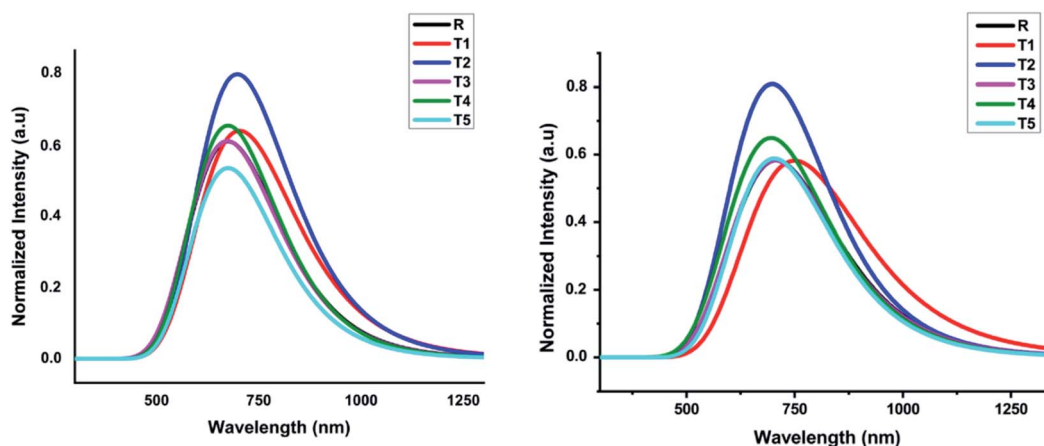

Fig. 7 Calculated absorption spectrum of all designed molecules (**T1–T5**) and reference **R** at TD-B3LYP/6-31G (d,p) in gas and solvent (**THF**) phases, respectively.
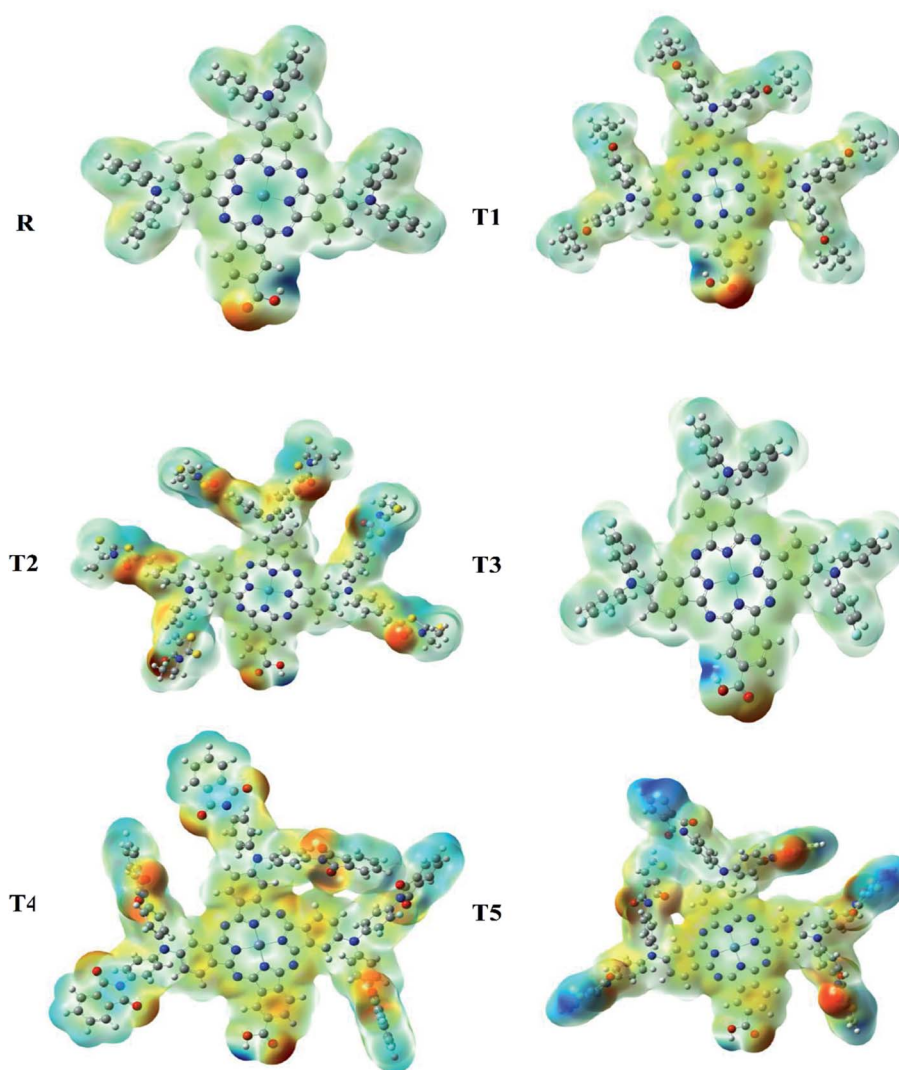
Fig. 8 Molecular electrostatic potential analysis of designed (T1–T5) and reference R molecules.

B3LYP at 6-31G (d,p) DFT method and are given in Table S1.† All molecules have greater dipole moments in **THF** solvent than the gaseous phase in the order of **T1** > **T5** > **R** > **T4** > **T3** > **T2**. The order of dipole moment in the gaseous phase is **T1** > **T5** > **R** > **T4** > **T2** > **T3**. In the gaseous phase, dipole moment values obtained

are reference **R** (8.510861 eV), **T1** (11.874998 eV), **T2** (5.861444 eV), **T3** (6.941926 eV), **T4** (7.053962 eV), and **T5** (9.05621 eV). The dipole moment values of reference **R** and compounds **T1–T5** are 10.007204, 14.073258, 8.515336, 8.468785, 8.762656, and 10.919255 eV, respectively, given in Fig. 9.

The **T2** molecule has a lower dipole moment in gaseous and solvent phases than the four designed (**T1, T3, T4, T5**) and reference molecule **R**, confirming their higher stability in organic solar cell devices. The higher values of the dipole moments allow the self-assembly of all designed molecules and the formation of long chains that provide a strong route for the transfer of charge. The dipole moment in excited (μ_e), ground (μ_g), and the difference (μ_e–μ_g) between these two states are given in Table S1,† respectively.

Open circuit voltage

To calculate the effectiveness of dye sensitized solar cells, open-circuit voltage is the main feature and relates to the competency of the device. The open-circuit voltage of any substance shows the biased junction of current lost from the organic solar cells.[30]

Table 3 Reorganization energies of reference R and designed molecules T1–T5

Molecules	$\lambda_e{}^a$ (eV)	$\lambda_h{}^b$ (eV)
R	0.19217	0.08712
T1	0.19631	0.06297
T2	0.14933	0.07883
T3	0.19986	0.08122
T4	0.07197	0.10100
T5	0.20844	0.12448

^{a} Reorganization energy of the electron. ^{b} Reorganization energy of the hole.
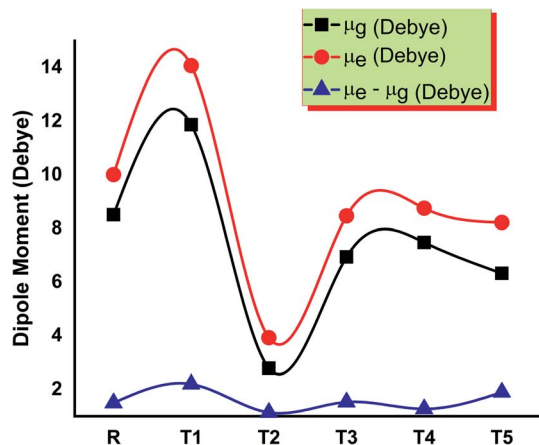
Fig. 9 Comparison of the dipole moment of designed molecules T1–T5 and reference R.

Usually, open circuit voltage initiates from zero and is used to calculate the recombination amount in organic solar cells. The open-circuit voltage can be calculated by eqn (3).[31]

$$V_{oc} = \frac{1}{e}\left(E^{D}_{HOMO} - E^{A}_{LUMO}\right) - 0.3 \qquad (3)$$

Here, e is the elementary charge. The value of open-circuit voltage is calculated by the difference between the E_{LUMO} of the acceptor and E_{HOMO} of the donor of the molecule. Furthermore, this difference in the energy of HOMO and LUMO is directly related to the open-circuit voltage. The designed molecules (T1–T5) are the donors and are suitable to manufacture OPV devices, and due to this reason, we compare our donor molecules with an acceptor molecule named PCBM (6,6-phenyl-C_{71}-butyric acid methyl ester).[32] The open-circuit voltage results obtained from eqn (3) with respect to $LUMO_{PC_{71}BM}$–$HOMO_{donor}$ energy gaps are represented in Fig. 10(a). The molecular orbital diagram shows the difference between the E_{HOMO} of donor compounds (T1–T5) and E_{LUMO} of the PCBM acceptor molecule.

The orbital energy of **R** and T1–T5 donors with respect to $PC_{71}BM$ acceptor are represented in Fig. 10 (b). The LUMO of $PC_{71}BM$ is less than the LUMO of donor molecules (**R, T1, T2, T3, T4,** and **T5**). This arrangement shifts the charge density
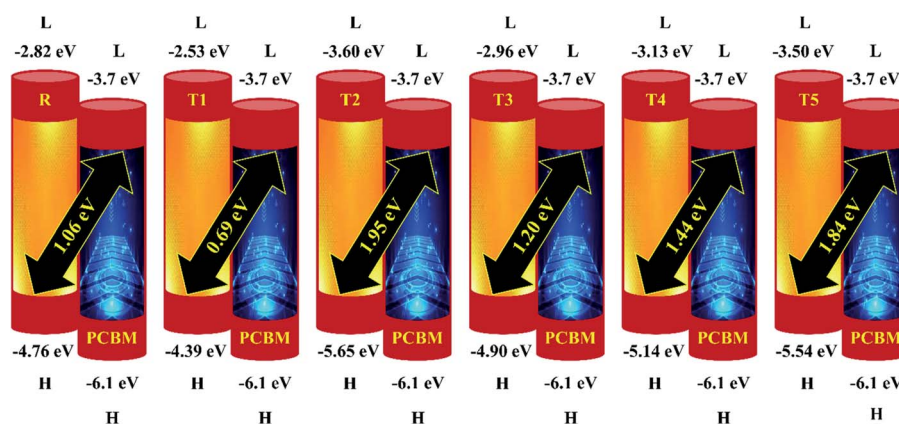
(a)
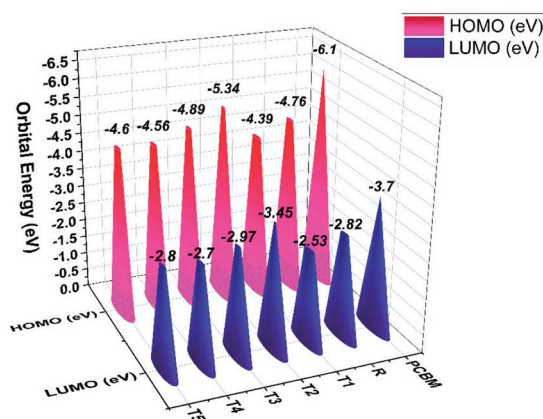
(b)

Fig. 10 (a) Open circuit voltage (V_{oc}) of designed donor molecules T1–T5 and reference R with respect to PC71BM acceptor, (b) orbital energy diagram of reference R and designed donor molecules T1–T5 with PC$_{71}$BM acceptor polymer.

from designed donor molecules (**T1, T2, T3, T4, T5**) to acceptor $PC_{71}BM$, which results in improved photovoltaic properties of all designed molecules.

Transition density matrix and exciton binding energy

The processes of electronic transitions are studied, analyzed, and interpreted by (TDMs) in dye-sensitized solar cells. TDM graphs give the characteristic 3D map between the two eigen states of the newly designed compounds. This 3D map represents associated electron–hole pair distribution and allows

them to recognize their lengths of coherence and delocalization.[33] TDM maps are largely used to explain the excitations of the transfer of charges in solar cells. To examine the emission and absorption up to ten excitation states of reference and other molecules (**T1–T5**), B3LYP/6-31G (d,p) functional and Multiwfn 3.7 software was used. The effect of hydrogen was neglected due to the negligible contribution of hydrogen atoms. The TDMs results are represented in Fig. 11.

TDM graphs are used to estimate (i) the process of excitations of electrons, (ii) delocalization and localization method of electron–hole pair, and (iii) interaction between the acceptor
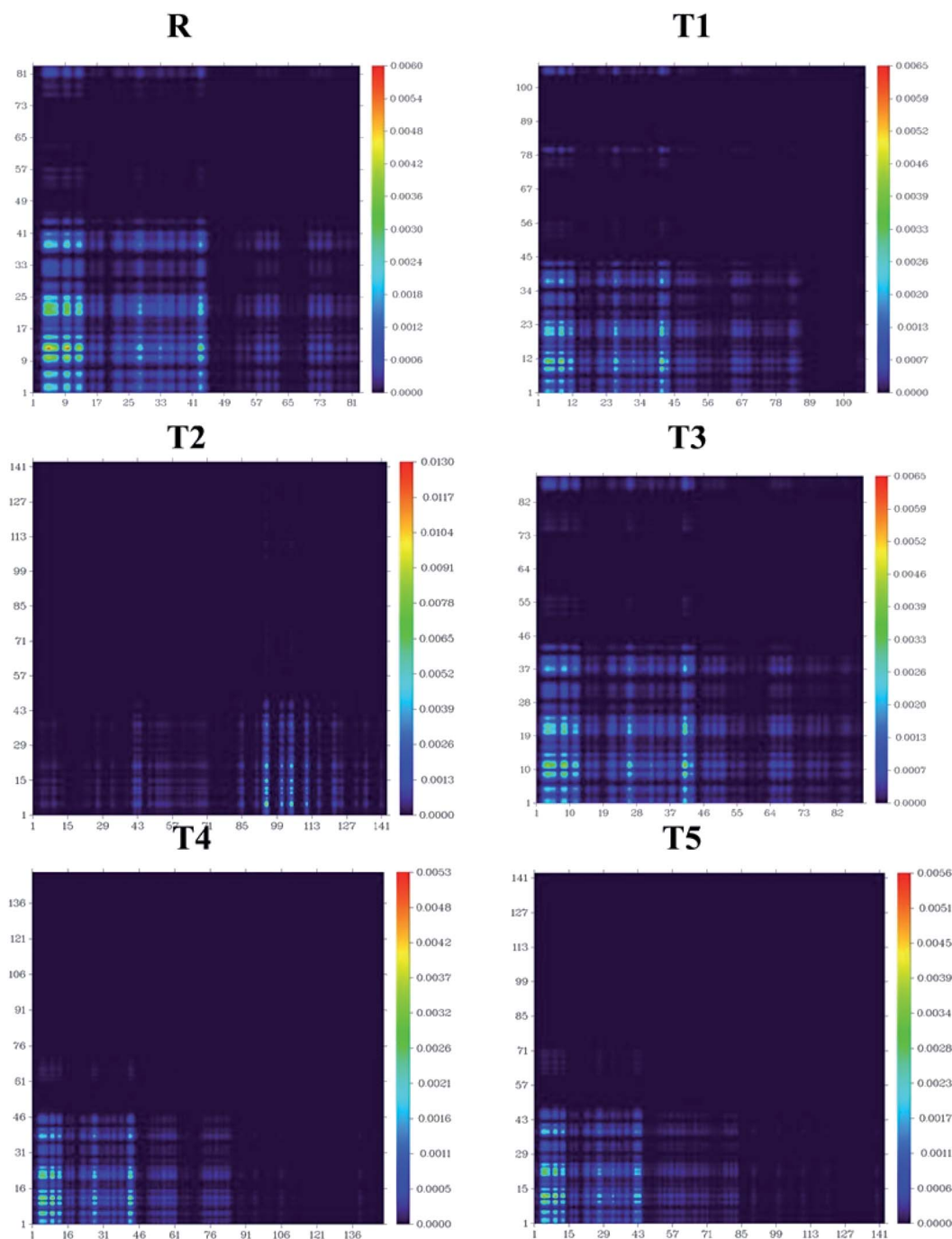

Fig. 11   TDMs of designed molecules **T1–T5** and reference molecule **R** in S_1 state.

and donor part of the molecule. We divide our designed compound into acceptor (A) and donor (D) part to evaluate the TDMs. The process of splitting of molecules **T1–T5** and reference is shown in Fig. 11. The transition density matrix map shows the coherence of electrons of **T1–T5** compounds and reference **R** having small coherence on acceptor parts and largely on donor moiety of the molecules. The order of interaction coefficients between acceptor and donor parts of molecules is **T1** > **T3** > **R** > **T5** > **T4** > **T2**. This order of interaction indicates that the coupling of electron and hole of **T1** is greater than other compounds.

In an excited state, because of the higher coupling value between the electron and hole (Fig. S2†), the **T1** molecule indicates harder and lower exciton dissociation. The values of binding energies show that molecule **T1** has the least light-harvesting capability and the least mobility of charges. Thus, the mobility of charges of **T1** is lower than all other compounds. The value of charge dissociation and J_{sc} (current charge density) for the **T2** molecule is higher than others. E_b (exciton binding energy) is a critical aspect of the rate of separation of charges and the efficiency of dye-sensitized solar cells. The bandgap is the difference of E_{HOMO} and E_{LUMO} values of molecular orbitals, and the optical gap (E_{opt}) is 1st excitation energy. The following equation[34] helps to calculate the binding energies of designed molecules **T1–T5** and reference **R**, theoretically.

$$E_b = E_g - E_{opt} \quad (4)$$

The analysis of exciton binding energies helps to measure the coulombic force of interaction between holes and electrons. The molecule having a low value of exciton binding energy shows low hole and electron interaction. In the first excited state, the **T2** molecule has a higher degree of separation of charges, which corresponds to lower E_b. **T2**, **T4**, and **T5** molecules have lower E_b values and correspond to a higher degree of charge separation. The order of exciton binding energy is **T2** < **T4** < **T5** < **R** < **T3** < **T1**. The detailed comparison between E_g, E_{opt} and E_b is represented in Fig. S3.†

Conclusion

In this report, five zinc phthalocyanine-based dyes (**T1–T5**) were designed and investigated for photovoltaic trends using DFT approaches. The UV-vis spectra of **T1–T5** molecules and reference **R** are simulated at the B3LYP/6-31G (d,p) method of DFT. **T1** molecule shows greater absorption in gaseous and **THF** solvent phases than all molecules. In **THF** solvent, its λ_{max} is 751.88 nm. Furthermore, the E_g value of **T1** is lower than **T2**, **T3**, **T4**, and **R**. The exciton binding energies and transition density matrix (TDM) studies indicate the high charge transfer rate because of the lower E_b for **T1–T5** than **R**. Open circuit voltage results are achieved with acceptor polymer PC$_{71}$BM. **T1** has a lower open-circuit voltage value while **T2–T5** molecules have greater open circuit voltage values than reference **R**. The V_{oc} values for **T1**, **T2**, **T3**, **T4**, and **T5** molecules are 0.69, 1.95, 1.20, 1.44, and 1.84 V, respectively. Lower reorganization energy values of **T1–T5** show high charge transfer than **R**. The molecule

T1 has lower hole mobility (0.06297 eV) than all other molecules. It is apparent from all discussions that our designed molecules (**T1**, **T2**, **T3**, **T4**, and **T5**) can be superb competitors for dye-sensitized solar cells.

Conflicts of interest

There are no conflicts to declare.

Acknowledgements

References

1 A. Hagfeldt, G. Boschloo, L. Sun, L. Kloo and H. Pettersson, Dye-sensitized solar cells, *Chem. Rev.*, 2010, **110**(11), 6595–6663, DOI: 10.1021/cr900356p.

2 C. P. Lee, *et al.*, Recent progress in organic sensitizers for dye-sensitized solar cells, *RSC Adv.*, 2015, **5**(30), 23810–23825, DOI: 10.1039/c4ra16493h.

3 N. Robertson, Catching the rainbow: Light harvesting in dye-sensitized solar cells, *Angew. Chem., Int. Ed.*, 2008, **47**(6), 1012–1014, DOI: 10.1002/anie.200704538.

4 G. De La Torre, C. G. Claessens and T. Torres, Phthalocyanines: Old dyes, new materials. Putting color in nanotechnology, *Chem. Commun.*, 2007, **20**, 2000–2015, DOI: 10.1039/b614234f.

5 M. E. Ragoussi and T. Torres, Modern synthetic tools toward the preparation of sophisticated phthalocyanine-based photoactive systems, *Chem.–Asian J.*, 2014, **9**(10), 2676–2707, DOI: 10.1002/asia.201402311.

6 M. V. Martínez-Díaz, G. De La Torre and T. Torres, Lighting porphyrins and phthalocyanines for molecular photovoltaics, *Chem. Commun.*, 2010, **46**(38), 7090–7108, DOI: 10.1039/c0cc02213f.

7 V. K. Singh, R. K. Kanaparthi and L. Giribabu, Emerging molecular design strategies of unsymmetrical phthalocyanines for dye-sensitized solar cell applications, *RSC Adv.*, 2014, **4**(14), 6970–6984, DOI: 10.1039/c3ra45170d.

8 M. Serhan, *et al.*, Total iron measurement in human serum with a smartphone, *AIChE Annu. Meet., Conf. Proc.*, 2019, **2019**, 1–3, DOI: 10.1039/x0xx00000x.

9 M. Batool, *et al.*, Study of biogenically fabricated transition metal oxides nanoparticles on oral cavity infectious microbial strains, *Inorg. Nano-Met. Chem.*, 2021, **51**(6), 856–866, DOI: 10.1080/24701556.2020.1811729.

10 M. Batool, S. Khurshid, W. M. Daoush, S. A. Siddique and T. Nadeem, Green synthesis and biomedical applications of ZnO nanoparticles: Role of pegylated-zno nanoparticles as doxorubicin drug carrier against MDA-MB-231(TNBC) Cells Line, *Crystals*, 2021, **11**(4), 344, DOI: 10.3390/cryst11040344.

11 P. Y. Reddy, *et al.*, Efficient Sensitization of Nanocrystalline TiO2 Films by a Near-IR-Absorbing Unsymmetrical Zinc

Phthalocyanine, *Angew. Chem.*, 2007, **119**(3), 377–380, DOI: 10.1002/ange.200603098.

12 J. J. Cid, *et al.*, Structure-function relationships in unsymmetrical zinc phthalocyanines for dye-sensitized solar cells, *Chem.–Eur. J.*, 2009, **15**(20), 5130–5137, DOI: 10.1002/chem.200801778.

13 M. García-Iglesias, *et al.*, Increasing the efficiency of zinc-phthalocyanine based solar cells through modification of the anchoring ligand, *Energy Environ. Sci.*, 2011, **4**(1), 189–194, DOI: 10.1039/c0ee00368a.

14 L. Giribabu, V. K. Singh, C. V. Kumar, Y. Soujanya, P. Y. Reddy and M. L. Kantam, Triphenylamine-phthalocyanine based sensitizer for sensitization of nanocrystalline TiO2 films, *Sol. Energy*, 2011, **85**(6), 1204–1212, DOI: 10.1016/j.solener.2011.02.027.

15 G. Tunç, E. Güzel, I. Şişman, V. Ahsen, G. Cárdenas-Jirón and A. G. Gürek, Effect of new asymmetrical Zn(ii) phthalocyanines on the photovoltaic performance of a dye-sensitized solar cell, *New J. Chem.*, 2019, **43**(36), 14390–14401, DOI: 10.1039/c9nj02585e.

16 E. Nouri, *et al.*, Soluble tetratriphenylamine Zn phthalocyanine as Hole Transporting Material for Perovskite Solar Cells, *Electrochim. Acta*, 2016, **222**, 875–880, DOI: 10.1016/j.electacta.2016.11.052.

17 M. Frisch, G. Trucks and H. Schlegel, *G. S.- Inc., W. CT, and undefined 2009*, "gaussian 09, Revision d. 01, Gaussian.

18 R. Dennington, T. Keith, A. J. Millam, *GaussView, Version 6*, Semichem Inc., Shawnee Mission, KS, 2016.

19 R. Milan, *et al.*, Dye-sensitized solar cells based on a push-pull zinc phthalocyanine bearing diphenylamine donor groups: Computational predictions face experimental reality, *Sci. Rep.*, 2017, **7**(1), 1–10, DOI: 10.1038/s41598-017-15745-3.

20 R. Hussain, *et al.*, Enhancement in Photovoltaic Properties of N,N-diethylaniline based Donor Materials by Bridging Core Modifications for Efficient Solar Cells, *ChemistrySelect*, 2020, **5**(17), 5022–5034, DOI: 10.1002/slct.202000096.

21 M. Bilal Ahmed Siddique, *et al.*, Designing Triphenylamine-Configured Donor Materials with Promising Photovoltaic Properties for Highly Efficient Organic Solar Cells, *ChemistrySelect*, 2020, **5**(25), 7358–7369, DOI: 10.1002/slct.202001989.

22 N. Ohta, K. Yamashita and A. Muraoka, Mechanism of charge transfer and separation in polymer/nonfullerene acceptor organic solar cells, *Bull. Am. Phys. Soc.*, 2020, **65**, 7148–7155, Accessed: Aug. 18, 2020. [Online]. Available: http://meetings.aps.org/Meeting/MAR20/Session/M71.84.

23 S. A. Siddique, *et al.*, Efficient tuning of triphenylamine-based donor materials for high-efficiency organic solar cells, *Comput. Theor. Chem.*, 2020, **1191**, 113045, DOI: 10.1016/j.comptc.2020.113045.

24 M. Akram, *et al.*, End-capped engineering of bipolar diketopyrrolopyrrole based small electron acceptor molecules for high performance organic solar cells, *Comput. Theor. Chem.*, 2021, **1201**, 113242, DOI: 10.1016/j.comptc.2021.113242.

25 M. Abbas, U. Ali, M. Faizan and M. B. A. Siddique, Spirofluorene based small molecules as an alternative to traditional non-fullerene acceptors for organic solar cells, *Opt. Quantum Electron.*, 2021, **53**(5), 1–14, DOI: 10.1007/s11082-020-02672-3.

26 P. Goszczycki, K. Stadnicka, M. Z. Brela, J. Grolik and K. Ostrowska, Synthesis, crystal structures, and optical properties of the π-π interacting pyrrolo[2,3-b]quinoxaline derivatives containing 2-thienyl substituent, *J. Mol. Struct.*, 2017, **1146**, 337–346, DOI: 10.1016/j.molstruc.2017.06.008.

27 J. S. Murray and P. Politzer, Molecular electrostatic potentials and noncovalent interactions, *Wiley Interdiscip. Rev.: Comput. Mol. Sci.*, 2017, **7**(6), e1326, DOI: 10.1002/wcms.1326.

28 N. Qiu, *et al.*, A New Nonfullerene Electron Acceptor with a Ladder Type Backbone for High-Performance Organic Solar Cells, *Adv. Mater.*, 2017, **29**(6), 1604964, DOI: 10.1002/adma.201604964.

29 M. Y. Mehboob, *et al.*, Designing N-phenylaniline-triazol configured donor materials with promising optoelectronic properties for high-efficiency solar cells, *Comput. Theor. Chem.*, 2020, **1186**, 112908, DOI: 10.1016/j.comptc.2020.112908.

30 J. Zhao, *et al.*, High-efficiency non-fullerene organic solar cells enabled by a difluorobenzothiadiazole-based donor polymer combined with a properly matched small molecule acceptor, *Energy Environ. Sci.*, 2015, **8**(2), 520–525, DOI: 10.1039/c4ee02990a.

31 M. C. Scharber, *et al.*, Design rules for donors in bulk-heterojunction solar cells - Towards 10 % energy-conversion efficiency, *Adv. Mater.*, 2006, **18**(6), 789–794, DOI: 10.1002/adma.200501717.

32 P. Mahendia, G. Chauhan and H. Wadhwa, Study of induced structural, optical and electrochemical properties of Poly (3-hexylthiophene)(P3HT),-phenyl-C61-butyric-acid-methyl-ester (PCBM) and their, *Elsevier*, 2020, **148**, 109644. Available: https://www.sciencedirect.com/science/article/pii/S002236971932147X.

33 M. U. Khan, M. Y. Mehboob, R. Hussain, Z. Afzal, M. Khalid and M. Adnan, Designing spirobifullerene core based three-dimensional cross shape acceptor materials with promising photovoltaic properties for high-efficiency organic solar cells, *Int. J. Quantum Chem.*, 2020, **120**(22), e26377, DOI: 10.1002/qua.26377.

34 M. E. Köse, Evaluation of acceptor strength in thiophene coupled donor-acceptor chromophores for optimal design of organic photovoltaic materials, *J. Phys. Chem. A*, Dec. 2012, **116**(51), 12503–12509, DOI: 10.1021/jp309950f.